

Geophysical Research Letters

RESEARCH LETTER

10.1029/2020GL091627

Key Points:

- Field-aligned H^+ beams are a systematic feature near Jupiter's main auroral emissions
- Potential structures >100 V transport 3 ± 2 kg s^{-1} of ionospheric H^+ from Jupiter to the middle and outer magnetosphere
- This phenomenon is a significant source of H^+ in Jupiter's magnetosphere

Correspondence to:

J. R. Szalay,
jszalay@princeton.edu










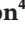

Citation:

Szalay, J. R., Allegrini, F., Bagenal, F., Bolton, S. J., Clark, G., Connerney, J. E. P., et al. (2021). Proton outflow associated with Jupiter's auroral processes. *Geophysical Research Letters*, 48, e2020GL091627. <https://doi.org/10.1029/2020GL091627>

Received 7 NOV 2020

Accepted 6 DEC 2020

Proton Outflow Associated With Jupiter's Auroral Processes

J. R. Szalay¹ , F. Allegrini^{2,3} , F. Bagenal⁴ , S. J. Bolton², G. Clark⁵ , J. E. P. Connerney^{6,7} , R. W. Ebert^{2,3} , R. E. Ergun⁴ , B. Mauk⁵ , D. J. McComas¹ , P. Valek² , and R. J. Wilson⁴ 

¹Department of Astrophysical Sciences, Princeton University, Princeton, NJ, USA, ²Southwest Research Institute, San Antonio, TX, USA, ³Department of Physics and Astronomy, University of Texas at San Antonio, San Antonio, TX, USA, ⁴Laboratory for Atmospheric and Space Physics, University of Colorado Boulder, Boulder, CO, USA, ⁵Applied Physics Laboratory, The Johns Hopkins University, Laurel, MD, USA, ⁶Space Research Corporation, Annapolis, MD, USA, ⁷Goddard Space Flight Center, Greenbelt, MD, USA

Abstract Field-aligned proton beams are a systematic and identifiable feature associated with Jupiter's auroral emissions, transporting 3 ± 2 kg s^{-1} away from Jupiter's ionosphere. This mass loss occurs at all longitudes sampled by Juno around the southern auroral oval, while the northern hemisphere exhibits upward proton beams predominantly on one portion in System III, near the auroral kink region. These beams are associated with upward inverted-V structures indicative of quasi-static magnetic field-aligned parallel potentials. A lack of bidirectionality indicates these proton populations are pitch-angle and/or energy scattered and incorporated into the magnetospheric charged particle environment. This mechanism is a significant, and potentially dominant, source of protons in Jupiter's middle and outer magnetosphere. If Jupiter's ionosphere is the primary source for protons in the inner magnetosphere, they are likely sourced equatorward of the main emissions and at energies <100 eV.

Plain Language Summary We find fluxes of narrow proton beams streaming away from Jupiter, where 3 ± 2 kg s^{-1} flows away from Jupiter's atmosphere into its local magnetic system. The mass loss occurs consistently around Jupiter's southern auroral emissions, but is not uniform in the northern hemisphere. These beams are found to be a significant source of protons for much of Jupiter's magnetic environment.

1. Introduction

The source of protons in the Jovian magnetosphere has been historically difficult to determine experimentally. The volcanic moon Io is the primary source of plasma in the magnetosphere, inputting $\sim 10^3$ kg s^{-1} of heavy ions (e.g., Bagenal & Delamere, 2011). Approximately 10% of the total magnetospheric number density is attributed to protons (e.g., Dougherty et al., 2017), which are not sourced by Io. The proton influx necessary to account for this population from 5 to 30 R_J (Jovian radii) has been estimated to be 2.5–13 kg s^{-1} (Bodisch et al., 2017).

There are at least three possible sources of protons in Jupiter's magnetosphere: solar wind, icy moons, and ionospheric outflow. Solar wind leakage across the magnetopause boundary is one possible source (e.g., Delamere et al., 2015), yet it is difficult to explain how such protons would be transported to the inner magnetosphere via this mechanism. Since Jupiter is likely not undergoing standard a Dungey cycle (McComas & Bagenal, 2007), it is also difficult to attribute magnetospheric protons to the solar wind, particularly in the inner-most regions. Of the icy moons, Europa sustains a neutral torus of many species including hydrogen (e.g., Smith et al., 2019), which can charge exchange with the local plasma environment, however, at much lower quantities than necessary to source the magnetospheric proton population (e.g., Bagenal & Dols, 2020). The focus of this study is to constrain the ionospheric outflow source of protons. The outflow has been previously estimated to be 35 kg s^{-1} (Nagy et al., 1986) integrating over the entire polar region, and 18.7–31.7 kg s^{-1} (Martin et al., 2020) at high latitudes between Io's M-Shell and up to and including the auroral oval, with 4.3–8.5 kg s^{-1} estimated to specifically outflow from the auroral oval. Both theoretical estimates are sufficient to explain the source of protons in Jupiter's magnetosphere, but the mechanisms of ionospheric outflow have not been previously observed.

To constrain ionospheric outflow, we analyze ion observations from two charged particle instruments on-board the Juno spacecraft (Bolton et al., 2017): JADE—the Jovian Auroral Distributions Experiment (McComas et al., 2017a) and JEDI—the Jupiter Energetic Particle Detector Instrument (Mauk et al., 2017a). The JADE instrument suite comprises two electron instruments (JADE-E) and one ion time-of-flight (TOF) mass spectrometer (JADE-I). The JEDI instrument suite contains two instruments capable of measuring both ions and electrons (J090 and J270) and one instrument set to measure only electrons (J180). In Jupiter's polar magnetosphere, JADE-I has made direct measurements of the ionosphere (Valek et al., 2019), observed discrete regions with separate ion and electron characteristics (Szalay et al., 2017), and found evidence for proton acceleration associated with Io's Alfvénic interaction with the magnetosphere (Szalay et al., 2020). JEDI ion observations near the polar region have revealed both upward and downward proton beams (Mauk et al., 2017c, 2018, 2020), proton conics with much larger energies than their terrestrial counterparts (Clark et al., 2017), constrained energetic heavy ion charge states (Clark et al., 2020), and revealed an auroral environment with both similarities and significant differences to Earth's (Mauk et al., 2017c). JADE and JEDI observations have enabled the characterization of identifiable auroral zones (Allegrini et al., 2020; Mauk et al., 2020), generally organized by latitude. One of Juno's important discoveries is that Jupiter's auroral emissions can be generated (a) during mono-directional, downward acceleration—Zone I: thought to be the upward electric current region and (b) during bidirectional electron acceleration—Zone II: thought to be the downward electric current region (Mauk et al., 2020).

Here, we analyze 21 distinct observations of upward proton beams simultaneously observed across JADE and JEDI's energy range. In Section 2, we describe the broad characteristics of these beams. In Section 3, we provide a statistical analysis across all observations and conclude with a discussion in Section 4.

2. Identification of H⁺ Beams

Due to the differences in orientation between the JADE-I and JEDI detectors, field-aligned proton beams are more readily observed by JADE-I so long as they occur within its energy range of 10 eV–50 keV. JEDI's J090 and J270 detectors are mounted to Juno such that their FOV is nearly aligned with Juno's spin plane (Mauk et al., 2017). The J090 and J270 sensors utilize a TOF and solid-state detector energy system to measure the velocity and total energy of the incident ions for clean compositional measurements. Although J180, by design, can make similar measurements, this sensor is operated in an “energy-only” mode where TOF measurements of the ions are not made. Therefore, while JEDI can attain higher time resolution with its spin-plane mounted detectors, they can only detect field-aligned proton beams when the magnetic field is nearly perpendicular to Juno's spin vector. JADE-I on the other hand is mounted with an FOV perpendicular to the Juno spin plane and is able to sample all viewing directions in 4π at least once per spin (McComas et al., 2017a, 2017b, 2017c). This comes at the sacrifice of temporal resolution, as it often only samples field-aligned populations for a short duration once or twice within a 30 s spin. While JADE-I can detect protons >10 eV, we restrict our analysis to >100 eV to avoid cold populations (e.g., Valek et al., 2019) near Juno's ram speed of $\sim 40\text{--}50\text{ km s}^{-1}$.

Figure 1 shows a representative example proton beam observed by JADE. The top two subpanels show proton differential energy intensity ($\text{cm}^{-2}\text{ sr}^{-1}\text{ s}^{-1}$) and pitch angle from JADE-I, while the bottom two subpanels show the same quantities for electrons from JADE-E. Pitch angles include protons with energies >100 eV and are determined using the onboard broadcast magnetic field vector from the MAG instrument (Connerney et al., 2017) which is returned with JADE data. Figure 1a shows the entire portion of the 9th Juno perijove in the southern hemisphere (PJ9S) auroral transit, mapping from the inner edge of the Io torus (Szalay et al., 2017) out to poleward of the main emissions, with all quantities spin-averaged. Figure 1b shows a zoomed in portion of the proton beam at JADE's native resolution of 1 s for electrons and 2 s for protons. Gray regions show where JADE could not observe certain pitch angles. The diffuse, Zone I, and Zone II auroral regions (Mauk et al., 2020) are identified at the top of Figure 1. The dashed line indicates where the Zone I boundary was less definitive and the solid line for Zone I also corresponds to the main emission boundaries according to Allegrini et al. (2020).

Some key signatures are exhibited in Figure 1. In the spin-averaged Figure 1a, an enhancement is observed in the upward loss cone with protons, indicating proton outflow, particularly in the region denoted

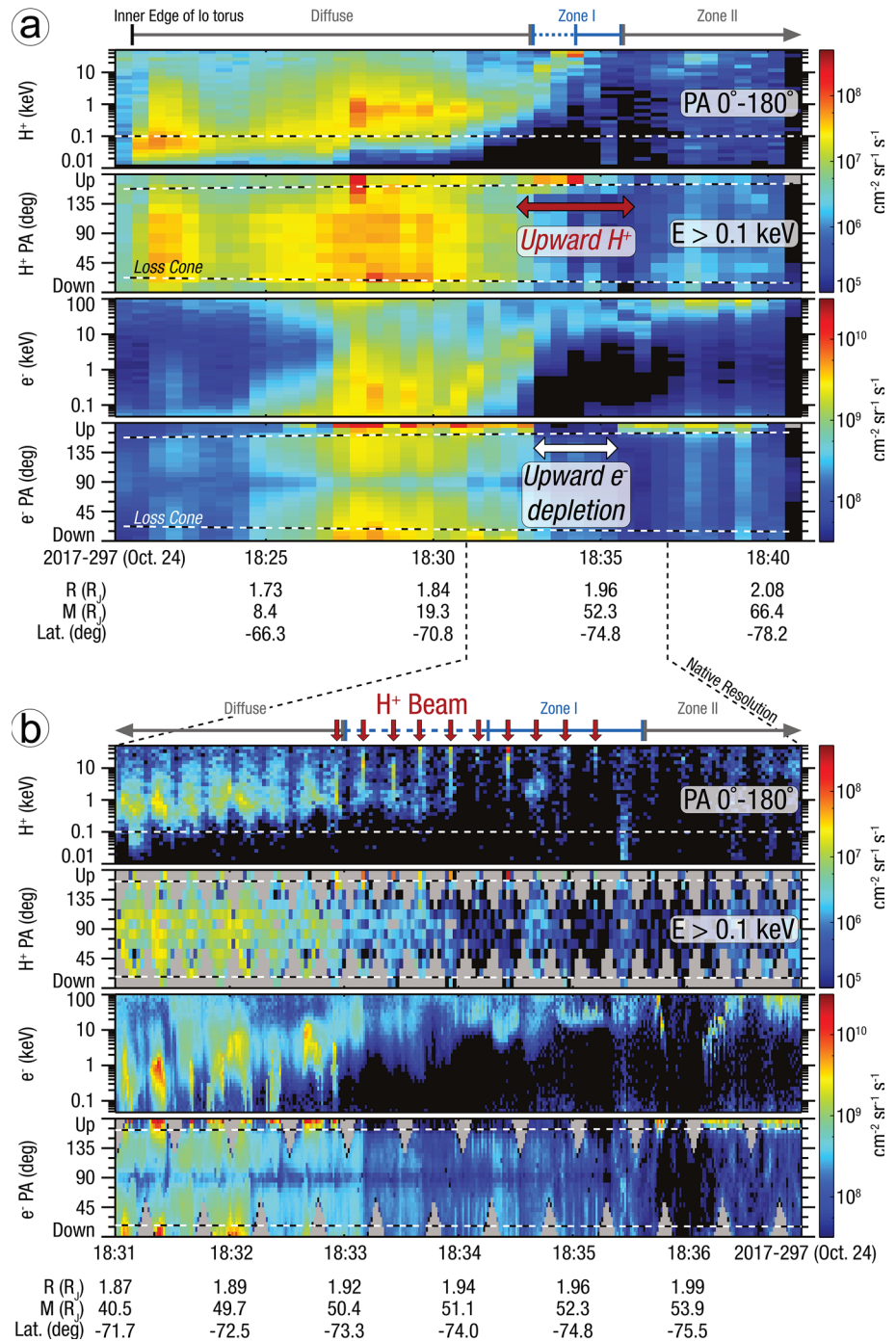


Figure 1. Proton beam observed by JADE during PJ9 South for spin-averaged (a) and native (b) resolution. The top two subpanels show proton differential energy intensity and pitch angle, while the bottom two subpanels show the same quantities for electrons. Energy spectrograms are for the full range of pitch angles (dashed lines indicate the loss cone) and proton pitch angle spectrograms are for $E > 0.1$ keV, marked with the dashed line in the first subpanel.

with “Upward H^+ ” in red. Contemporaneously, a depletion of upward electrons is observed, indicating the process accelerating the protons upward is also preventing electrons from reaching Juno from Jupiter. As shown in Figure 1b for JADE’s native time resolution, proton beams are observed only when JADE-I directly looks toward the upward field-aligned direction, here twice per spin. The beams are very narrow

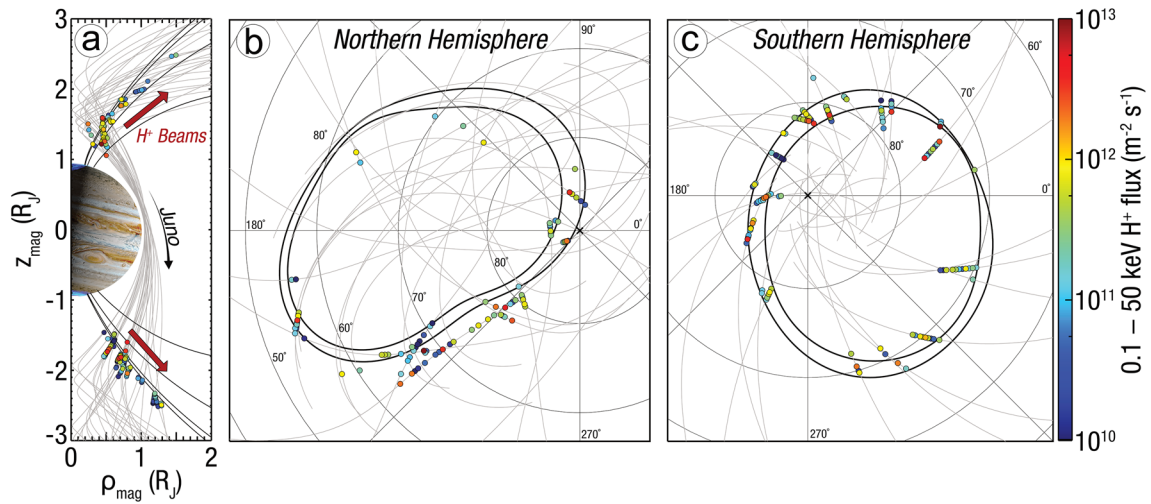


Figure 2. H^+ total number flux below 50 keV each time it was identified in JADE data, propagated to the atmosphere. (a) Trajectory and field lines in magnetic dipole coordinates, (b) in orthographic projection, northern hemisphere, and (c) orthographic projection southern hemisphere. Gray lines show the magnetic footprint along the Juno trajectory. Black lines in (a) correspond to M-Shells of 5, 10, 20, and 40 R_J , and to the statistical average boundaries of the UV main emissions in (b) and (c).

in angular extent, typically detected during a single time step and in the most field-aligned pitch angle bin corresponding to anti-planetward moving protons.

3. Observation Geometry and H^+ Beam Trends

Given the observational differences between JADE and JEDI, we first identify proton beams in the JADE-I data by searching each perijove for the features described in the previous section. Figure 2 shows all times identified within the JADE data up to and including PJ28. Colors correspond to the average flux within the upward loss cone, assuming an area-projection weighted size of the loss cone above Jupiter's atmosphere of π (Mauk et al., 2017). Juno's trajectory mapped to the atmosphere is shown in gray. Figure 2a is given in the Juno VIP4 dipole frame (Connerney et al., 1998), with magnetic field lines mapping to equatorial M-Shell values of 5, 10, 20, and 40 R_J . Figures 2b and 2c show the auroral projection in System III coordinates, mapped to the Jovian atmosphere, along with the average statistical boundaries of the auroral ovals (Bonfond et al., 2012). The statistical oval shown is one representation of the main emissions and are intended to be a reference, not a strict boundary for the location of the main emissions. We use the JRM09 magnetic field model (Connerney et al., 2018) along with a modeled magnetodisk current sheet (Connerney et al., 1981) to map along the magnetic field.

Key trends for the proton beams are shown in Figure 2. Figure 2a shows beams are typically confined to a specific range of latitudes/M-Shells. In the northern hemisphere (Figure 2b), upward beams are not observed every transit across the main oval and the large majority of detections occur near the auroral kink region. In contrast, proton beams are observed for every southern hemisphere transit and occur within or just poleward of the average location of the main emissions.

Figure 3 shows four examples that illustrate the different characters found for these beams. The top subpanel shows the JADE ($<50 \text{ keV}$) and JEDI ($>50 \text{ keV}$) differential energy intensities within the upward loss cone. The second and third subpanels show pitch angle spectrograms for JEDI (50–2,600 keV) and JADE (0.1–50 keV) in differential number intensity. The last subpanel shows total upward number flux for JEDI (red), JADE (blue), and the total (black). Vertical dashed lines show the region identified as the relevant inverted-V shaped structures in the spectrograms, used to calculate the total Jovian proton mass flux estimates contained in these beams.

Figure 3a shows the PJ9S example given in Figure 1. Here, a well-organized and asymmetric (with respect to time) inverted-V is observed, which begins at or below 0.1 keV and extends up to nearly 1 MeV. The peak mass flux occurs for energies around 100 keV and spans both the JADE and JEDI energy ranges. This transit

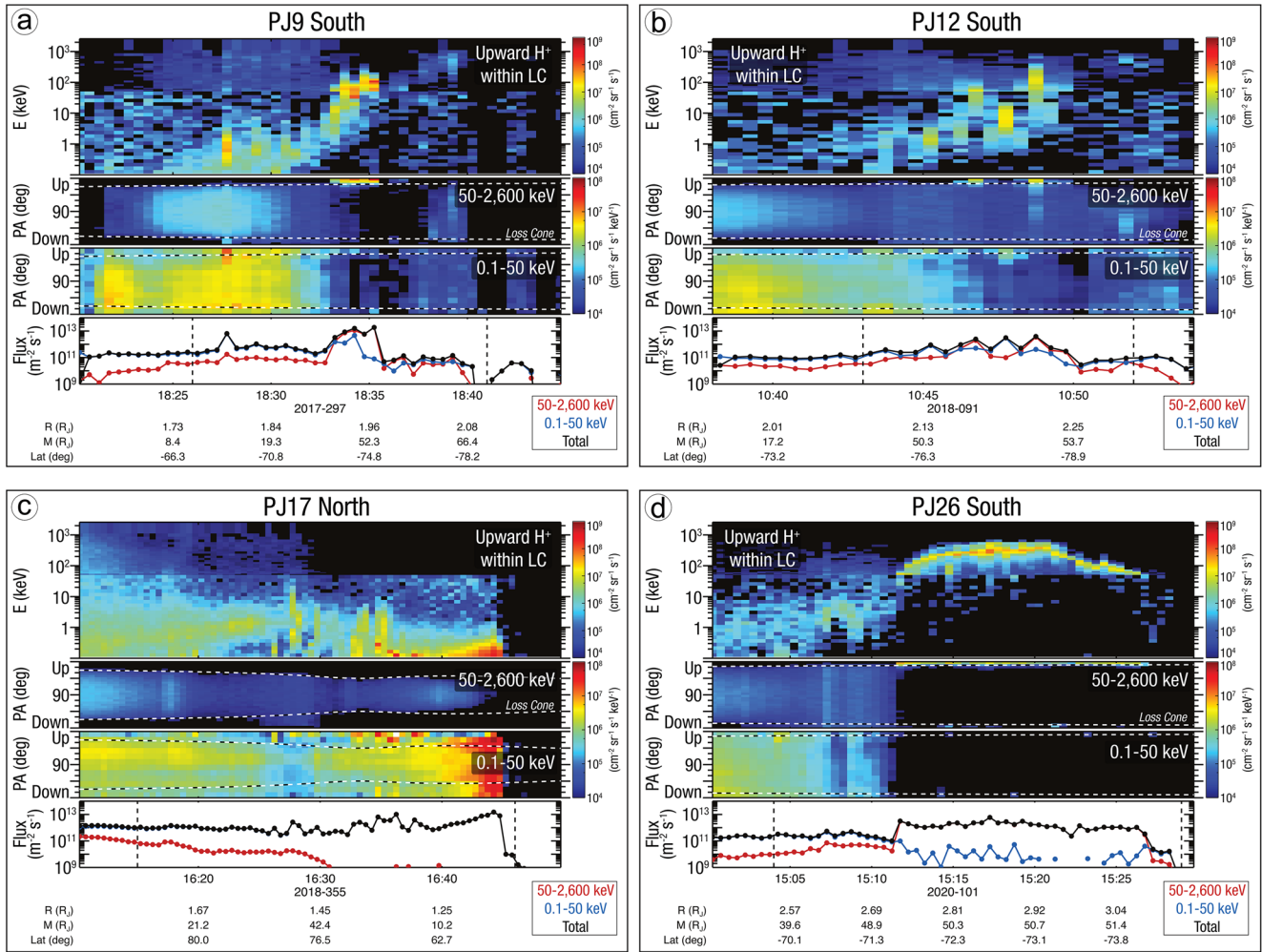


Figure 3. Upward H^+ beam observations for found representative transits. Subpanels show differential energy intensity for both JADE and JEDI (top), differential number intensity pitch angle (middle) for JEDI (50–2,600 keV) and JADE (0.1–50 keV) and total upward number flux (bottom) for JADE (blue), JEDI (red), and combined (black).

also exhibits a small upward flux enhancement at lower latitudes for protons ~ 1 keV around 18:27. Figure 3b shows another asymmetric inverted-V during the southern PJ12 transit (PJ12S) with significantly more variation in energy intensity structure, where the peak intensity occurs at nonmonotonically changing energies over consecutive time steps as shown in the top panel. The energy carrying the dominant mass flux also alternates between JADE's and JEDI's energy ranges.

Figure 3c shows a lower latitude instance in the northern hemisphere for PJ17N. Here, Juno never fully transits the statistical main emissions, skirting them in more equatorial latitudes near the northern kink region. The vast majority of upward proton mass flux occurs below 10 keV. Figure 3d shows the most organized and symmetric inverted-V for upward proton beams in the southern hemisphere. Here, the mass flux is dominantly observed in JEDI's energy range, peaking ~ 400 keV. The lower energy boundaries of the inverted-V are observable in JADE's energy range, extending down to sub-keV levels on either side.

These four cases exemplify the types of features observed during upward proton beam measurements. Table 1 gives relevant parameters for the 21 crossings analyzed in this work. We note that many more crossings were observed in the JADE data that were omitted from this table due to the limited available pitch angles for JEDI later in the mission; statistical analysis is performed on beams where both instruments were able to observe the upward loss cone.

Table 1
Table of All Upward Proton Beams With Both a Signal in JADE and JEDI

PJ	DOY	t_0	t_1	Alt ₀ (R _J)	Alt ₁ (R _J)	Lat ₀ (deg)	Lat ₁ (deg)	Width (km)	Percent < 50 keV	Total (kg s ⁻¹ m ⁻¹)
1 N	2016–240	12:09:00	12:17:00	0.76	0.59	81.4	71.0	9,800	92	1.9×10^{-8}
1 S	2016–240	13:26:00	13:39:00	0.62	0.93	−67.4	−79.2	10,300	90	1.4×10^{-8}
3 S	2016–346	17:33:00	17:39:00	0.48	0.62	−65.6	−69.6	8,500	97	1.3×10^{-8}
4 S	2017–033	13:35:00	13:40:00	0.68	0.80	−77.0	−77.0	4,700	43	5.7×10^{-9}
5 S	2017–086	09:36:00	09:49:00	0.82	1.14	−72.7	−85.4	9,300	29	2.6×10^{-8}
6 N	2017–139	05:27:00	05:34:00	0.59	0.43	70.9	62.0	6,700	99	6.1×10^{-9}
6 S	2017–139	06:47:00	07:00:00	0.87	1.19	−74.3	−87.1	8,100	92	8.4×10^{-9}
7 N	2017–192	01:14:00	01:21:00	0.75	0.59	87.2	77.5	10,200	75	4.5×10^{-8}
7 S	2017–192	02:29:00	02:36:00	0.59	0.75	−63.4	−72.1	7,800	65	4.6×10^{-9}
8 S	2017–244	22:25:00	22:30:00	0.63	0.75	−71.5	−71.5	5,600	74	2.0×10^{-9}
9 S	2017–297	18:26:00	18:41:00	0.81	1.17	−77.3	−81.6	11,200	30	4.1×10^{-8}
10 N	2017–350	17:22:00	17:29:00	0.62	0.46	75.9	65.2	9,900	99	9.5×10^{-8}
11 N	2018–038	12:55:00	12:59:00	1.13	1.03	88.3	87.3	1,600	85	2.1×10^{-9}
12 N	2018–091	09:05:00	09:12:00	0.75	0.59	86.7	79.4	4,700	78	1.3×10^{-8}
12 S	2018–091	10:43:00	10:52:00	1.14	1.36	−80.5	−86.0	3,500	48	4.9×10^{-9}
14 N	2018–197	04:40:00	04:47:00	0.67	0.51	85.8	79.4	8,900	82	3.6×10^{-8}
16 N	2018–302	20:11:00	20:18:00	1.09	0.92	77.8	75.2	3,800	93	8.9×10^{-9}
17 N	2018–355	16:15:00	16:46:00	0.85	0.20	79.8	48.3	12,200	99	4.1×10^{-8}
18 N	2019–043	16:45:00	16:55:00	0.96	0.72	77.7	75.7	7,100	48	1.2×10^{-8}
23 N	2019–307	21:52:00	21:57:00	0.42	0.32	68.5	61.9	2,100	100	1.1×10^{-8}
26 S	2020–101	15:04:00	15:29:00	1.61	2.19	−81.7	−83.6	2,800	7.5	5.3×10^{-8}

Altitudes are given from relative to the nominal oblate Jovian spheroid (flattening = 15.4), latitudes are given in System III, width is measured perpendicular to the average auroral oval, the percentage of flux below 50 keV calculated as the fluxes in the JADE energy range 0.1–50 keV divided by the total flux across the JADE and JEDI energy ranges given in the last column.

The last column of Table 1 lists the mass flux per unit length, determined by taking the average upward mass flux between the time boundaries in Table 1 and multiplying by feature width mapped to Jupiter's atmosphere in the direction perpendicular to the main oval (“width” in Table 1).

To calculate total mass loss from Jupiter, we take the average upward proton mass flux per unit length perpendicular to the auroral oval (Table 1) for each hemisphere and multiply by the appropriate arclength along the auroral oval track. In the northern hemisphere, we use a truncated length of 6×10^4 km near the kink region (~30% of the entire track), while we use the entire auroral track length of 1.2×10^5 km in the south. From this, we estimate a proton outflow rate of 3 ± 2 kg s⁻¹ due to this process.

4. Discussion and Conclusions

Upward proton beams are a systematic feature near Jupiter's main auroral emissions. These beams are organized in classic “inverted-V” signatures, indicative of quasi-static parallel potentials driving their acceleration. A lack of bidirectionality indicates these populations are pitch-angle and/or energy scattered, likely via wave-particle interactions, and incorporated into the magnetospheric charged particle populations. Such a mechanism has been previously observed at Earth (e.g., Shelley et al., 1976; Yau & André, 1997), where parallel potential structures simultaneously accelerate electrons planetward to generate auroral emissions and produce anti-planetward ion beams as a source of ionospheric material to the magnetosphere (Ergun

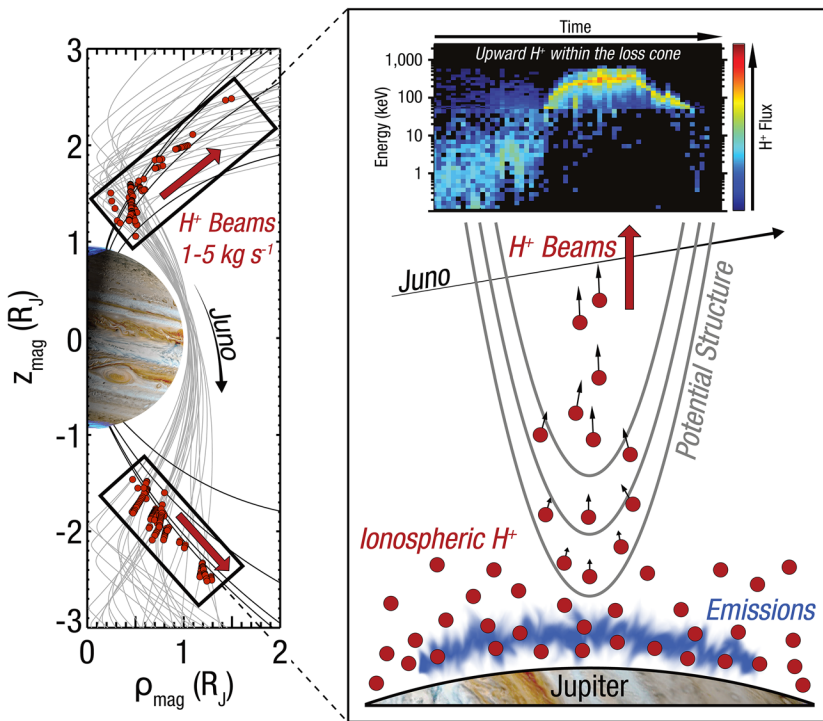


Figure 4. Schematic showing potential structures that accelerate ionospheric protons away from Jupiter. This process manifests as “inverted-V’s” in the charged particle data.

et al., 2001, 2002a, 2002b, 2004). Multiple transit geometries and observations have occurred at Earth, consistent with parallel potential acceleration: (a) above the main acceleration region (upward ion beams), (b) in the middle of the acceleration region (both downward electron and upward ion beams), and (c) below the acceleration regions (downward electron beams). The observations discussed here exhibit many similar features. Figure 4 shows a summary schematic of this process at Jupiter, where potential structures access the proton population in Jupiter’s ionosphere.

The specific phenomena discussed in this work injects $1\text{--}5\text{ kg s}^{-1}$ of protons into Jupiter’s magnetosphere and is likely a lower bound. The beam widths are approximately $10\text{--}20^\circ$, and narrower than the currently used JADE-I geometric factor, which assumes a warm population. Constraining the exact correction factor to adjust for a narrow beam would require extensive forward modeling of the instrument response; we estimate the actual mass loss could be on the order of a factor of two higher than reported here. If the total mass flux required to sustain the Jovian proton population is $2.5\text{--}13\text{ kg s}^{-1}$ (Bodisch et al., 2017), these beams are a significant, if not dominant, source of protons. While beams are observed on field lines that typically map to equatorial distances past 50 R_J for the assumed current sheet used in this analysis (Connerney et al., 1981), updates to this model likely decrease these

equatorial distance estimates (Connerney et al., 2020). Phenomenologically, since this process is associated with the main auroral emissions, it is likely injecting protons into Jupiter’s middle and outer magnetosphere from $\sim 20\text{ R}_J$ and above.

While these beams are not likely the source of protons in the inner-most portions of the magnetosphere, they may be an important contribution toward explaining observations of protons dominating the dawn-side of the outer magnetosphere (McComas et al., 2017c) and far down the magnetotail (McComas et al., 2007, 2017b). If Jupiter is the primary source of magnetospheric protons in the inner magnetosphere (within $\sim 20\text{ R}_J$), they are likely sourced at latitudes equatorward of the main emissions and at lower energies than 100 eV discussed in this work, which would also explain why these estimates are on the lower end of previous ionospheric mass fluxes (Nagy et al., 1986; Martin et al., 2020). The mass outflow found here of $1\text{--}5\text{ kg s}^{-1}$ is consistent with the values of $4.3\text{--}8.5\text{ kg s}^{-1}$ predicted to occur within a nominal 2° main oval (Martin et al., 2020). While Juno has made direct observations of ionospheric H^+ at latitudes between the main emissions and Io’s orbital footprint (Valek et al., 2019) and near the equator (Valek et al., 2020), thus far it has been difficult to constrain the ionospheric outflow rate in situ.

Proton fluxes are found to vary orbit-by-orbit and indicate potential structures may be both spatially and/or temporally varying. The bulk of the acceleration occurs below the spacecraft altitude of $0.2\text{--}2.0\text{ R}_J$ (Table 1) and the feature widths perpendicular to the statistical main auroral oval, magnetically mapped to Jupiter’s atmosphere, vary from $2,000$ to $12,000\text{ km}$. The energy of the potential structures is not correlated to the total mass flux or altitude. The available mass flux is likely driven by how much ionospheric material is accessible to the potential structures. Analogous terrestrial outflows were found to be due to both dissipation of downward Poynting flux and electron heating from precipitating electron fluxes (Strangeway et al., 2005). The majority of the acceleration sustaining this mass loss occurs for potentials under 50 keV (Table 1).

These observations indicate the presence of broad potential structures predicted to be connected to Jupiter’s main emissions and associated upward current regions (e.g., Cowley & Bunce, 2001; Hill, 2001). While these structures have been posited to power the main emissions, stochastic Alfvénic acceleration has also been shown to be a key

component of Jupiter's auroral emissions (Saur et al., 2018). Signatures for both quasi-static and broadband (e.g., Alfvénic) acceleration have been observed by Juno connected to Jupiter's main emission (e.g., Mauk et al., 2020). In this work, we focus on the mechanisms responsible for Jupiter's ionospheric proton outflow. While these mechanisms are also important in understanding Jupiter's auroral emissions, they are one facet of the complex auroral processes occurring at Jupiter. We do not estimate auroral currents here, as this requires a detailed analysis of magnetic field observations that is beyond the scope of this work (e.g., Kotsiaros et al., 2019).

The potential structures responsible for accelerating protons are likely more complex than the simple schematic shown in Figure 4, as the peak mass flux is not always associated with the peak acceleration potential. Some signatures are particularly coherent and organized (e.g., PJ26S, Figure 3d), while other signatures show variations in peak energy flux even along the inverted-V signatures (PJ12S, Figure 3b). The peak mass fluxes are typically correlated with depletions in upward-going electrons (e.g., Figure 1), yet oftentimes they are bounded by regions with both upward electron and proton fluxes. Upward proton beams are typically, but not always, associated with Zone I auroral signatures (Mauk et al., 2020), which characteristically have downward energetic electron acceleration. A separate comparison between the determination of main emissions via in-situ electron fluxes (Allegrini et al., 2020) also suggests these proton beams occur near the main emissions. A lack of observed upward electrons near the peak upward mass flux indicates the acceleration region was at a low altitude, completely below the spacecraft, such that upward-going electrons were prevented from transiting through the potential barrier below. The potential structures may be temporally/spatially varying in altitude, have substantial substructure themselves, and/or the ionospheric scale height has significant local variations.

Proton mass loss occurs around the entire southern hemisphere, while the northern hemisphere sheds protons predominantly near the auroral kink region. The lack of beams in specific regions of the northern hemisphere may be related to the northern magnetic anomaly (Grodent et al., 2008), where magnetic fields are asymmetrically larger in the northern hemisphere compared to the southern hemisphere (Connerney et al., 2018). This process is operating efficiently near the “kink” in the northern main oval. Hence, such potential structures, if they exist, do not occur at low enough altitudes to access the reservoir of ionospheric H^+ or the ionospheric heating is less intense outside the kink region.

4.1. Summary

- Field-aligned H^+ beams are a systematic and identifiable feature associated with Jupiter's main auroral emissions
- Potential structures from ~ 100 eV up to 100 keV transport 3 ± 2 kg s^{-1} of ionospheric H^+ from Jupiter to the middle and outer magnetosphere
- These protons are pitch-angle and/or energy scattered and incorporated into the magnetospheric charged particle populations
- Ionospheric loss via this mechanism occurs around the entire southern hemisphere, while predominantly occurring near the auroral kink region the northern hemisphere
- This phenomenon is a significant source of magnetospheric H^+
- If Jupiter's ionosphere is the primary source for protons in the inner magnetosphere, they are likely shed from latitudes equatorward of the main emissions and at energies < 100 eV

Acknowledgments

We thank the many JADE, JEDI, and Juno team members that made these observations possible. We also thank M. Imai for producing the JRM09 magnetic field line integrations and B. Bonfond for the Jupiter image used in Figure 4. The JNO-J/SW-JAD-3-CALIBRATE-ED-V1.0 data set was obtained from the Planetary Data System (PDS) at <https://pds.nasa.gov/>. We acknowledge Juno's NASA contract NNM06AA75C.

References

- Allegrini, F., Mauk, B., Clark, G., Gladstone, G. R., Hue, V., Kurth, W. S., et al. (2020). Energy flux and characteristic energy of electrons over Jupiter's main auroral emission. *Journal of Geophysical Research: Space Physics*, 125, e2019JA027693. <https://doi.org/10.1029/2019JA027693>
- Bagenal, F., & Delamere, P. A. (2011). Flow of mass and energy in the magnetospheres of Jupiter and Saturn. *Journal of Geophysical Research*, 116, A05209. <https://doi.org/10.1029/2010JA016294>
- Bagenal, F., & Dols, V. (2020). The Space environment of Io and Europa. *Journal of Geophysical Research: Space Physics*, 125, 8241–8257. <https://doi.org/10.1029/2019JA027485>
- Bodisch, K. M., Dougherty, L. P., & Bagenal, F. (2017). Survey of voyager plasma science ions at Jupiter: 3. Protons and minor ions. *Journal of Geophysical Research: Space Physics*, 122, 8277–8294. <https://doi.org/10.1002/2017JA024148>
- Bolton, S. J., Lunine, J., Stevenson, D., Connerney, J. E. P., Levin, S., Owen, T. C., et al. (2017). The Juno mission. *Space Science Reviews*, 213(1–4), 1–33. <https://doi.org/10.1007/s11214-017-0429-6>
- Bonfond, B., Grodent, D., Gérard, J.-C., Stallard, T., Clarke, J. T., Yoneda, M., (2012). Auroral evidence of Io's control over the magnetosphere of Jupiter. *Geophysical Research Letters*, 39, L01105. <https://doi.org/10.1029/2011GL050253>

- Clark, G., Mauk, B. H., Kollmann, P., Paranicas, C. P., Bagenal, F., Allen, R. C., et al. (2020). Heavy ion charge states in Jupiter's polar magnetosphere inferred from auroral megavolt electric potentials. *Journal of Geophysical Research: Space Physics*, 125, e2020JA028052. <http://doi.org/10.1029/2020JA028052>
- Clark, G., Mauk, B. H., Paranicas, C. P., Haggerty, D., Kollmann, P., Rymer, A., et al. (2017). Observation and interpretation of energetic ion conics in Jupiter's polar magnetosphere. *Geophysical Research Letters*, 44, 4419–4425. <http://doi.org/10.1002/2016GL072325>
- Connerney, J. E. P., Acuna, M. H., Ness, N. F., & Satoh, T. (1998). New models of Jupiter's magnetic field constrained by the Io flux tube footprint. *Journal of Geophysical Research*, 103(A6), 11929–11939. <https://doi.org/10.1029/97JA03726>
- Connerney, J. E. P., Acuna, M. H., & Ness, N. F. (1981). Modeling the Jovian current sheet and inner magnetosphere. *Journal of Geophysical Research*, 86(A10), 8370–8384. <https://doi.org/10.1029/JA086iA10p08370>
- Connerney, J. E. P., Benn, M., Bjarno J. O., Denver T., Espley J., Jorgensen J. L., et al. (2017). The Juno magnetic field investigation. *Space Science Reviews*, 213, 39–138. <http://doi.org/10.1007/s11214-017-0334-z>
- Connerney, J. E. P., Kotsiaros, S., Oliverson, R. J., Espley J. R., Joergensen J. L., Joergensen P. S., et al. (2018). A new model of Jupiter's magnetic field from Juno's first nine orbits. *Geophysical Research Letters*, 45, 2590–2596. <http://doi.org/10.1002/2018GL077312>
- Connerney, J. E. P., Timmins, S., Hecceg, M., & Joergensen, J. L. (2020). A Jovian magnetodisc model for the Juno era. *Journal of Geophysical Research: Space Physics*, 125, e2020JA028138. <http://doi.org/10.1029/2020JA028138>
- Cowley, S. W. H., & Bunce, E. J. (2001). Origin of the main auroral oval in Jupiter's coupled magnetosphere-ionosphere system. *Planetary and Space Science*, 49(1), 1067–1088. [http://doi.org/10.1016/S0032-0633\(00\)00167-7](http://doi.org/10.1016/S0032-0633(00)00167-7)
- Delamere, P. A., Bagenal, F., Paranicas, C. P., Masters, A., Radioti, A., Bonfond, B., et al. (2015). Solar wind and internally driven dynamics: Influences on magnetodiscs and auroral responses. *Space Science Reviews*, 187, 1–47. <http://doi.org/10.1007/s11214-014-0075-1>
- Dougherty, L. P., Bodisch, K. M., & Bagenal, F. (2017). Survey of voyager plasma science ions at Jupiter: 2. Heavy ions. *Journal of Geophysical Research: Space Physics*, 122, 8257–8276. <http://doi.org/10.1002/2017JA024053>
- Ergun, R. E., Andersson, L., Main, D. S., Su, Y. J., Carlson, C. W., McFadden, J. P., & (2002a). Parallel electric fields in the upward current region of the aurora: Indirect and direct observations. *Physics of Plasmas*, 9(9), 3685–3694. <http://doi.org/10.1063/1.1499120>
- Ergun, R. E., Andersson, L., Main, D., Su, Y. J., Newman, D. L., Goldman, M. V., et al. (2002b). Parallel electric fields in the upward current region of the aurora: Numerical solutions. *Physics of Plasmas*, 9(9), 3695–3704. <http://doi.org/10.1063/1.1499121>
- Ergun, R. E., Andersson, L., Main, D., Su, Y. J., Newman, D. L., Goldman, M. V., et al. (2004). Auroral particle acceleration by strong double layers: The upward current region. *Journal of Geophysical Research*, 109, A12220. <http://doi.org/10.1029/2004JA010545>
- Ergun, R. E., Su, Y. J., Andersson, L., Carlson, C. W., McFadden, J. P., Mozer, F. S., et al. (2001). Direct observation of localized parallel electric fields in a Space plasma. *Physical Review Letters*, 87(4), 292–294. <http://doi.org/10.1103/PhysRevLett.87.045003>
- Grodent, D., Bonfond, B., Gérard, J.-C., Radioti, A., Gustin, J., Clarke, J. T., et al. (2008). Auroral evidence of a localized magnetic anomaly in Jupiter's northern hemisphere. *Journal of Geophysical Research*, 113, A09201. <http://doi.org/10.1029/2008JA013185>
- Hill, T. W. (2001). The Jovian auroral oval. *Journal of Geophysical Research*, 106(A5), 8101–8108. <http://doi.org/10.1029/2000JA000302>
- Kotsiaros, S., Connerney, J. E. P., Clark, G., Allegrini, F., Gladstone, G. R., Kurth, W. S., et al. (2019). Birkeland currents in Jupiter's magnetosphere observed by the polar-orbiting Juno spacecraft. *Nature Astronomy*, 3(10), 904–909. <http://doi.org/10.1038/s41550-019-0819-7>
- Martin, C. J., Ray, L. C., Constable, D. A., Southwood, D. J., Lorch, C. T. S., & Felici, M. (2020). Evaluating the ionospheric mass source for Jupiter's magnetosphere: An ionospheric outflow model for the auroral regions. *Journal of Geophysical Research: Space Physics*, 125, e2019JA027727. <http://doi.org/10.1029/2019JA027727>
- Mauk, B. H., Clark, G., Gladstone, G. R., Kotsiaros, S., Adriani, A., Allegrini, F., et al. (2020). Energetic particles and acceleration regions over Jupiter's polar cap and main aurora: A broad overview. *Journal of Geophysical Research: Space Physics*, 125, e2019JA027699. <http://doi.org/10.1029/2019JA027699>
- Mauk, B. H., Haggerty, D. K., Jaskulek, S. E., Schlemm, C. E., Brown, L. E., Cooper, S. A., et al. (2017a). The Jupiter energetic particle detector instrument (JEDI) investigation for the Juno mission. *Space Science Reviews*, 213(1–4), 289–346. <https://doi.org/10.1007/s11214-013-0025-3>
- Mauk, B. H., Haggerty, D. K., Paranicas, C. P., Clark, G., Kollmann, P., Rymer, A. M., et al. (2017b). Juno observations of energetic charged particles over Jupiter's polar regions: Analysis of monodirectional and bidirectional electron beams. *Geophysical Research Letters*, 44, 4410–4418. <http://doi.org/10.1002/2016GL072286>
- Mauk, B. H., Haggerty, D. K., Paranicas, C. P., Clark, G., Kollmann, P., Rymer, A. M., et al. (2017c). Discrete and broadband electron acceleration in Jupiter's powerful aurora. *Nature*, 549(7670), 66–69. <http://doi.org/10.1038/nature23648>
- Mauk, B. H., Haggerty, D. K., Paranicas, C., Clark, G., Kollmann, P., Rymer, A. M., et al. (2018). Diverse electron and ion acceleration characteristics observed over Jupiter's main aurora. *Geophysical Research Letters*, 45, 1277–1285. <https://doi.org/10.1002/2017GL076901>
- McComas, D. J., Alexander, N., Allegrini, F., Bagenal, F., Beebe, C., Clark, G., et al. (2017a). The Jovian auroral Distributions experiment (JADE) on the Juno mission to Jupiter. *Space Science Reviews*, 213(1–4), 547–643. <https://doi.org/10.1007/s11214-013-9990-9>
- McComas, D. J., Allegrini, F., Bagenal, F., Cray, F., Ebert, R. W., Elliott, H., (2007). Diverse plasma populations and structures in Jupiter's magnetotail. *Science*, 318, 217. <http://doi.org/10.1126/science.1147393>
- McComas, D. J., Allegrini, F., Bagenal, F., Ebert, R. W., Elliott, H. A., Nicolaou, G., et al. (2017b). Jovian deep magnetotail composition and structure. *Journal of Geophysical Research: Space Physics*, 121, 1763–1777. <http://doi.org/10.1002/2016JA023039>
- McComas, D. J., & Bagenal, F. (2007). Jupiter: A fundamentally different magnetospheric ***interaction with the solar wind. *Geophysical Research Letters*, 34, 421–425. <http://doi.org/10.1029/2007GL031078>
- McComas, D. J., Szalay J. R., Allegrini F., Bagenal F., Connerney J., Ebert R. W., et al. (2017c). Plasma environment at the dawn flank of Jupiter's magnetosphere: Juno arrives at Jupiter. *Geophysical Research Letters*, 44, 4432–4438. <https://doi.org/10.1002/2017GL072831>
- Nagy, A. F., Barakat, A. R., & Schunk, R. W. (1986). Is Jupiter's ionosphere a significant plasma source for its magnetosphere? *Journal of Geophysical Research*, 91(A1), 351–354. <http://doi.org/10.1029/JA091iA01p00351>
- Saur, J., Janser, S., Schreiner, A., Clark, G., Mauk, B. H., Kollmann, P., et al. (2018). Wave-particle interaction of Alfvén waves in Jupiter's magnetosphere: Auroral and magnetospheric particle acceleration. *Journal of Geophysical Research: Space Physics*, 123, 9560–9573. <http://doi.org/10.1029/2018JA025948>
- Shelley, E. G., Sharp, R. D., & Johnson, R. G. (1976). Satellite observations of an ionospheric acceleration mechanism. *Geophysical Research Letters*, 3(11), 654–656. <http://doi.org/10.1029/GL003i011p00654>
- Smith, H. T., Mitchell, D. G., Johnson, R. E., Mauk, B. H., & Smith, J. E. (2019). Europa neutral torus confirmation and characterization based on observations and modeling. *The Astrophysical Journal*, 871(1), 69. <http://doi.org/10.3847/1538-4357/aad38>
- Strangeway, R. J., Ergun, R. E., Su, Y. J., Carlson, C. W., & Elphic, R. C. (2005). Factors controlling ionospheric outflows as observed at intermediate altitudes. *Journal of Geophysical Research*, 110, A03221. <http://doi.org/10.1029/2004JA010829>
- Szalay, J. R., Bagenal, F., Allegrini, F., Bonfond, B., Clark, G., Connerney, J. E. P., et al. (2020). Proton acceleration by Io's Alfvénic interaction. *Journal of Geophysical Research: Space Physics*, 125, e2019JA027314. <https://doi.org/10.1029/2019JA027314>

- Szalay, J. R., Allegrini F., Bagenal F., Bolton S., Clark G., Connerney J. E. P., et al. (2017). Plasma measurements in the Jovian polar region with Juno/JADE. *Geophysical Research Letters*, 44, 7122–7130. <http://doi.org/10.1002/2017GL072837>
- Valek, P. W., Allegrini, F., Bagenal, F., Bolton, S. J., Connerney, J. E. P., Ebert, R. W., et al. (2019). Jovian high-latitude ionospheric ions: Juno in situ observations. *Geophysical Research Letters*, 46, 8663–8670. <https://doi.org/10.1029/2019GL084146>
- Valek, P. W., Bagenal, F., Ebert, R. W., Allegrini, F., McComas, D. J., Szalay, J. R., et al. (2020). Juno in situ observations above the Jovian equatorial ionosphere. *Geophysical Research Letters*, 47, e2020GL087623. <https://doi.org/10.1029/2020GL087623>
- Yau, A. W., & André, M. (1997). Sources of ion outflow in the high latitude ionosphere. *Space Science Reviews*, 80(1), 1–25. <http://doi.org/10.1023/A:1004947203046>